nature chemical biology

BRIEF COMMUNICATION

PUBLISHED ONLINE: 14 SEPTEMBER 2014 | DOI: 10.1038/NCHEMBIO.1631

Arylquins target vimentin to trigger Par-4 secretion for tumor cell apoptosis

Ravshan Burikhanov[1,9], Vitaliy M Sviripa[2,3,9], Nikhil Hebbar[4], Wen Zhang[2,5], W John Layton[6], Adel Hamza[7], Chang-Guo Zhan[3,7,8], David S Watt[2,3,5,6], Chunming Liu[2,5] & Vivek M Rangnekar[1,4,5]*

The tumor suppressor protein prostate apoptosis response-4 (Par-4), which is secreted by normal cells, selectively induces apoptosis in cancer cells. We identified a 3-arylquinoline derivative, designated Arylquin 1, as a potent Par-4 secretagogue in cell cultures and mice. Mechanistically, Arylquin 1 binds vimentin, displaces Par-4 from vimentin for secretion and triggers the efficient paracrine apoptosis of diverse cancer cells. Thus, targeting vimentin with Par-4 secretagogues efficiently induces paracrine apoptosis of tumor cells.

Lung cancer is the most frequently diagnosed cancer and the leading cause of cancer-related deaths in the world[1]. Lung tumor cells with p53 mutations or deletions often develop resistance to chemotherapy and radiation therapy, leading ultimately to the death of the patients[2–4]. Notably, such p53-deficient cancer cells are susceptible to apoptosis by the proapoptotic tumor suppressor Par-4 (refs. 5–7). Par-4 induces apoptosis in diverse cancer cells but not in normal cells[7]. Par-4 is ubiquitously expressed in normal cells and tissues, but it is inactivated, downregulated or mutated in several types of cancers[7–9]. Both intracellular and secreted Par-4 have a role in apoptosis induction by caspase-dependent mechanisms[7]. Par-4 is secreted in cell culture–conditioned medium (CM) or systemically in mice from normal cells, and extracellular Par-4 binds its receptor GRP78 on the cancer cell surface and induces apoptosis[5,6]. In contrast, normal cells express low to undetectable levels of basal or inducible cell-surface GRP78 and are resistant to apoptosis by extracellular Par-4 (refs. 5,6).

Because the baseline levels of Par-4 secreted by normal cells are generally inadequate to cause massive apoptosis in cancer cell cultures, secretagogues that bolster the release of Par-4 constitute an important therapeutic advance. Nutlin-3a, originally developed as an MDM2 inhibitor[10], stimulated Par-4 secretion at micromolar levels in mouse embryonic fibroblast (MEF) cells[11]. The presence of halogen substituents on an aromatic ring, two aromatic rings separated by a two-atom spacer (i.e., a 1,2-diphenylethane subunit) and a nitrogen-containing heterocycle (i.e., an imidazole subunit) in Nutlin-3a enabled us to screen an in-house library that had similar features, namely halogenated aromatic rings separated by two-atom spacers (i.e.,1,2-diphenylethene or stilbene subunits) and nitrogen-containing heterocycles. Specifically, we focused on halogenated 3-arylquinolines, 3-arylquinolones and 3-arylthioquinolones, which had stilbene subunits and nitrogen-containing heterocyclic rings imbedded within their structures. A stilbene subunit imbedded within a 3-arylquinoline, for example, is highlighted in **Supplementary Results**, **Supplementary Note**. We screened representative members of each of these heterocyclic families on a compound-by-compound basis for the secretion of Par-4 protein from normal MEFs under conditions that were not toxic to

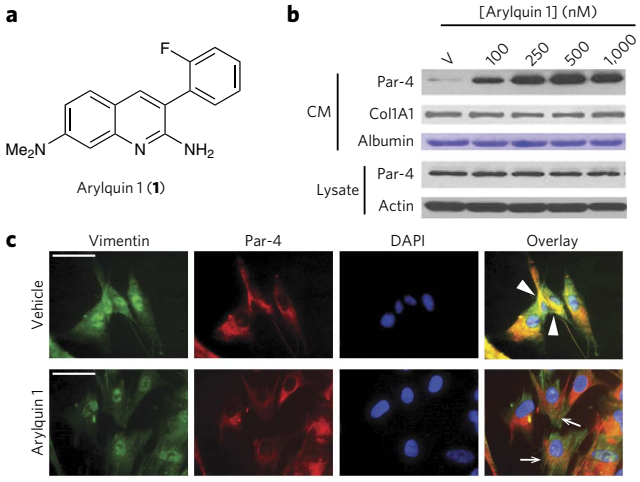

Figure 1 | Arylquin 1 displaces Par-4 bound to vimentin to induce Par-4 secretion. (**a**) Chemical structure of Arylquin 1. Arylquin 1 contains 2-amino and 7-(*N*,*N*-dimethyl)amino substituents on the quinoline ring and an *ortho*-fluorine on the C3 aryl group. (**b**) Arylquin 1 induces dose-dependent secretion of Par-4. MEF cells were treated with the indicated concentrations of Arylquin 1 or vehicle (V), and the amount of Par-4 in the CM or whole-cell lysate was quantified by western blot analysis. Albumin or collagen 1A1 in the CM or intracellular β-actin in the lysate served as a loading control. Uncut gels for **Figure 1b** can be found in **Supplementary Figure 17**. (**c**) Par-4 co-localizes with vimentin and is displaced from vimentin by Arylquin 1 treatment of cells. HEL cells, treated with vehicle or Arylquin 1 (500 nM) for 24 h, were subjected to ICC for Par-4 (red fluorescence) and vimentin (green fluorescence). Cells were stained with DAPI to reveal their nuclei (cyan fluorescence). Colocalization of Par-4 and vimentin in the overlay images shown in the vehicle panel is indicated by arrowheads (yellow fluorescence), and dissociation of Par-4 and vimentin (loss of yellow fluorescence with retention of red and green fluorescence) is indicated by arrows in the Arylquin 1 panel. Scale bars, 20 μm.

[1]Department of Radiation Medicine, College of Medicine, University of Kentucky, Lexington, Kentucky, USA. [2]Department of Molecular and Cellular Biochemistry, College of Medicine, University of Kentucky, Lexington, Kentucky, USA. [3]Center for Pharmaceutical Research and Innovation, College of Pharmacy, University of Kentucky, Lexington, Kentucky, USA. [4]Graduate Center for Toxicology, College of Medicine, University of Kentucky, Lexington, Kentucky, USA. [5]Lucille Parker Markey Cancer Center, University of Kentucky, Lexington, Kentucky, USA. [6]Department of Chemistry, College of Arts and Sciences, University of Kentucky, Lexington, Kentucky, USA. [7]Department of Pharmaceutical Sciences, College of Pharmacy, University of Kentucky, Lexington, Kentucky, USA. [8]Molecular Modeling and Biopharmaceutical Center, College of Pharmacy, University of Kentucky, Lexington, Kentucky, USA. [9]These authors contributed equally to this work. *e-mail: vmrang01@email.uky.edu

the cells. Initial expectations were that these heterocycles would serve as Nutlin-3a surrogates and inhibit MDM2, but studies reported herein established a completely different mechanism of action (**Supplementary Fig. 1**), reflecting that the structural dissimilarities between these heterocycles and Nutlin-3a outweighed the similarities that led to their initial selection for screening.

Within this library of compounds, the fluorinated 3-arylquinolines proved particularly promising in promoting Par-4 secretion. Structure-activity studies defined that 3-arylquinolines, such as Arylquin 1 (**1**) (**Fig. 1a** and **Supplementary Fig. 2**), were most active as the leading member of a new class of 'small-molecule' Par-4 secretagogues. Arylquin 1 produced a dose-dependent secretion in MEF cells (**Fig. 1b**). Arylquin 1 also induced robust secretion of Par-4 in normal or immortalized human cells but failed to induce the secretion of Par-4 in a panel of lung tumor cells (**Supplementary Fig. 3**). By contrast, prostate cancer cells showed induction of Par-4 secretion with Arylquin 1 treatment relative to vehicle control treatment (**Supplementary Fig. 3**). Consistent with previous studies[5], Brefeldin A, which blocked anterograde endoplasmic reticulum–Golgi traffic, inhibited basal as well as Arylquin 1–inducible Par-4 secretion (**Supplementary Fig. 3**). These findings indicated that Arylquin 1 regulated Par-4 secretion via the classical secretory pathway.

To identify the molecular target responsible for the observed Par-4 secretory activity, we synthesized a biotinylated Arylquin 9 (**9**; **Supplementary Note**). Biotinylated Arylquin 9 was confirmed experimentally to retain Par-4 secretory properties (**Supplementary Fig. 4**) and was then used in pulldown experiments for potential protein targets in MEFs and human fibroblast (HEL) cells. We identified vimentin, a cytoskeletal intermediate filament protein[12], as its principal target (**Supplementary Figs. 5** and **6**). The binding of Par-4 to vimentin was experimentally confirmed by co-immunoprecipitation experiments: the Par-4 antibody co-immunoprecipitated endogenous vimentin, and the vimentin antibody co-immunoprecipitated endogenous Par-4 (**Supplementary Fig. 7**). Immunocytochemical analysis confirmed that Par-4 co-localized with vimentin (**Fig. 1c**). In contrast, cells treated with Arylquin 1 showed neither Par-4 co-immunoprecipitation (**Supplementary Fig. 7**) nor colocalization (**Fig. 1c**) with vimentin, indicating that Arylquin 1 displaced Par-4 from vimentin. This action of Arylquin 1 was not associated with inhibition of vimentin expression (**Supplementary Fig. 8**), suggesting that Arylquin 1 may cause conformational changes in vimentin to inhibit its ability to bind and sequester Par-4 or compete for a hydrophobic binding region on vimentin crucial for Par-4 binding. The differential regulation of Par-4 secretion in normal and various cancer cells by Arylquin 1 (**Supplementary Fig. 3**) may reflect distinct post-translational modification patterns of Par-4, vimentin or both; studies are under way to address the underlying mechanism.

Computer modeling using molecular dynamics simulations led to a minimum-energy structure in which Arylquin 1 binds tetrameric vimentin in a hydrophobic pocket that lies between a pair of head-to-tail α-helical dimers (**Supplementary Fig. 9**). The spatial arrangement of functional groups within Arylquin 1 was ideally suited to stabilize binding to vimentin (**Supplementary Fig. 9**). Additional modeling revealed that Arylquin 1 and its analogs that have been examined bind vimentin in the same orientation but with different binding energies (**Supplementary Figs. 10–12**). The relative values of the calculated binding energies are qualitatively consistent with experimental trends: Arylquin 1, Arylquin 6 (**6**) and Arylquin 8 (**8**), which had the largest binding energies, promoted the highest levels of Par-4 secretion (**Supplementary Fig. 2** and **Supplementary Table 1**). The fluorine group in Arylquin 1 was indispensable for activity, and the removal of the fluorine was accompanied by reduced binding (**Supplementary Table 1**) and concomitant loss of Par-4 secretory activity (**Supplementary Fig. 2**).

Because targeting vimentin may induce apoptosis, we tested normal cells and diverse cancer cells for apoptosis by Arylquin 1. Arylquin 1 induced the dose-dependent apoptosis in cancer cells but not in normal cells (**Fig. 2a** and **Supplementary Fig. 13**). Notably, 500-nM amounts of Arylquin 1, which triggered secretion of Par-4 from normal cells but not lung cancer cells, did not directly induce apoptosis in normal or cancer cells. By contrast, 500-nM amounts of Arylquin 1 induced apoptosis of human prostate cancer (PC-3) cells and the derivative PC-3MM2 cells, which are sensitive to apoptosis by Par-4, but not in LNCaP or DU145 cells, which are resistant to apoptosis by Par-4 (refs. 5,6).

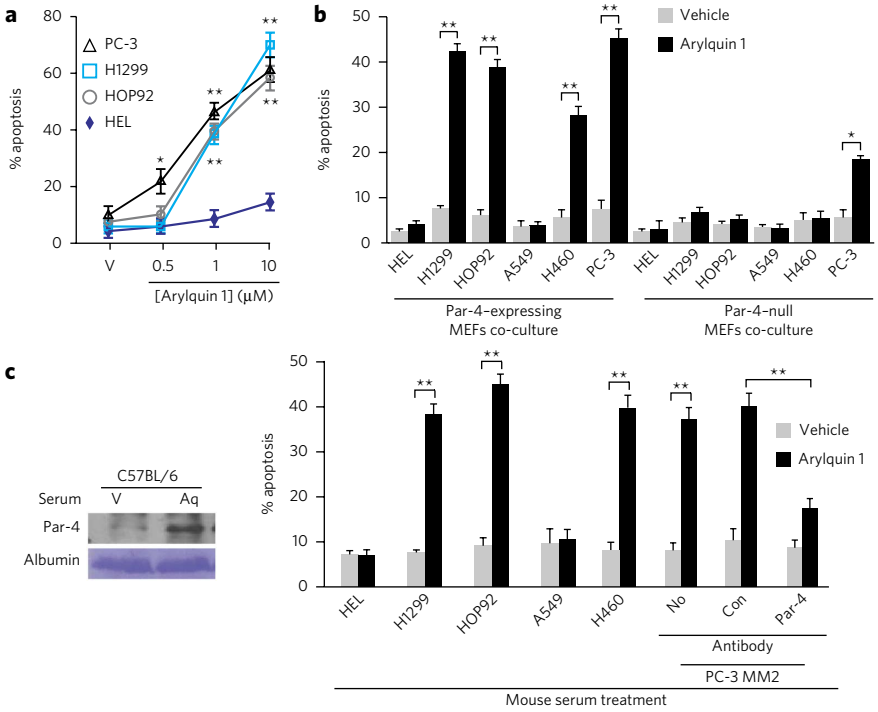

Figure 2 | Arylquin 1 induces paracrine apoptosis in cancer cells. (**a**) Arylquin 1 induces apoptosis. The indicated amounts of Arylquin 1 or vehicle (V) were added to the cells to test for apoptosis. (**b**) Arylquin 1 induces paracrine apoptosis. Cancer cells were cultured together with MEFs and treated with Arylquin 1 (500 nM) or vehicle and tested for apoptosis. (**c**) Arylquin 1 induces systemic Par-4 proapoptotic activity. Left, serum from C57BL/6 mice injected with Arylquin 1 (Aq) or corn oil vehicle (V) was examined by western blot analysis. Right, aliquots of serum from these mice were either directly added to the growth medium of cells in culture or incubated with the indicated antibody and then added to the growth medium of PC-3 MM2 cells to test for apoptosis. HEL cells are normal human lung fibroblasts, and H1299, HOP92, A549 and H460 are human cancer cell lines. No, no antibody; Con, control antibody; Par-4, Par-4 antibody. In **a**–**c**, Apoptotic cells were scored after 24 h, and data shown represent mean values from three independent experiments ±s.d. $*P < 0.001$ and $**P < 0.0001$, as measured by the Student *t*-test. Uncut gels for **Figure 2** can be found in **Supplementary Figure 18**.

We next tested co-cultures of normal cells with cancer cells for the apoptotic effect of Arylquin 1 at 500 nM, as this low concentration induced the secretion of Par-4 from normal cells yet did not induce apoptosis in normal or cancer cells. Arylquin 1 treatment of the co-cultures containing Par-4–expressing MEFs and cancer cells resulted in apoptosis of the cancer cells, in contrast with cells treated with vehicle (**Fig. 2b**). Only the cancer cells, and not normal HEL cells, underwent apoptosis in such co-culture experiments. By contrast, Arylquin 1 treatment of the co-cultures containing Par-4-null MEFs and cancer cells did not induce apoptosis. Paracrine apoptosis induced in the cancer cells by Par-4, which was secreted from Par-4–expressing MEFs but not Par-4–null MEFs in response to Arylquin 1 treatment (**Supplementary Fig. 14**), was mediated via cell-surface GRP78 (**Supplementary Fig. 15**). Moreover, vimentin-deficient cells[13,14] showed a robust increase in the secretion of proapoptotic Par-4 activity in the CM relative to their wild-type counterparts, and Arylquin 1 did not further induce Par-4 secretion in these cells (**Supplementary Fig. 16**). On the basis of these findings, we infer that (i) vimentin sequestered Par-4 and prevented its secretion and that (ii) Arylquin 1 bound vimentin and thereby altered the vimentin-Par-4 association to facilitate Par-4 secretion.

To determine the physiological significance of these findings, we injected immunocompetent mice with Arylquin 1 or vehicle and examined their serum for circulating levels of Par-4. Arylquin 1 treatment produced fivefold higher Par-4 secretion in serum relative to vehicle control treatment (**Fig. 2c**). Serum from the Arylquin 1–treated mice, but not vehicle-treated mice, produced significantly higher ($P < 0.001$) *ex vivo* apoptosis of cancer cell cultures (**Fig. 2c**). The proapoptotic activity in the serum was neutralized by the Par-4 antibody. These findings implied that systemic Par-4 levels were elevated in response to Arylquin 1 treatment and that these levels were effective in producing apoptosis of cancer cells.

In summary, the present study identified a new secretagogue, Arylquin 1, that produced a dose-dependent secretion of Par-4 at nanomolar concentrations from both normal fibroblasts and epithelial cells. Vimentin was the primary target of Arylquin 1, as determined using a biotinylated analog of Arylquin 1. Vimentin represents a particularly notable therapeutic target because of its elevation in diverse tumors and its causal role in EMT and metastasis[12]. Notably, this chemical genetics approach led to the identification of vimentin as a new binding partner of Par-4 and indicated that Arylquin 1 exhibited its function by binding vimentin and releasing vimentin-bound Par-4 for secretion. At low concentrations, Arylquin 1 by itself did not kill normal cells and most cancer cells, but instead it caused robust secretion of Par-4 from normal cells and triggered apoptosis in cancer cells only when they were used in co-culture experiments with normal cells. These findings, which implicated the secretion of Par-4 from normal cells in the apoptotic death of cancer cells, were corroborated by the observation that Arylquin 1 treatment of cancer cells co-cultured with Par-4–null normal cells failed to induce apoptosis of the cancer cells. Thus, Arylquin 1 induced paracrine apoptosis in cancer cells via Par-4 secreted by normal cells. Because Par-4 produced apoptosis in diverse tumors and because there were no previously reported compounds that acted at nanomolar concentrations to produce the levels of Par-4 secretion discovered in this study, these findings have potential translational significance.

Received 20 March 2014; accepted 13 August 2014; published online 14 September 2014

Methods

Methods and any associated references are available in the online version of the paper.

References

1. Siegel, R., Naishadham, D. & Jemal, A. *CA Cancer J. Clin.* **62**, 10–29 (2012).
2. Viallet, J. & Minna, J.D. *Am. J. Respir. Cell Mol. Biol.* **2**, 225–232 (1990).
3. Luo, S.Y. & Lam, D.C.L. *Transl. Respir. Med.* **1**, 6–8 (2013).
4. Chen, F., Wang, W. & El-Deiry, W.S. *Biochem. Pharmacol.* **80**, 724–730 (2010).
5. Burikhanov, R. *et al. Cell* **138**, 377–388 (2009).
6. Burikhanov, R. *et al. Cancer Res.* **73**, 1011–1019 (2013).
7. Hebbar, N., Wang, C. & Rangnekar, V.M. *J. Cell. Physiol.* **227**, 3715–3721 (2012).
8. Shrestha-Bhattarai, T., Hebbar, N. & Rangnekar, V.M. *Cancer Cell* **24**, 3–5 (2013).
9. Alvarez, J.V. *et al. Cancer Cell* **24**, 30–44 (2013).
10. Vassilev, L.T. *et al. Science* **303**, 844–848 (2004).
11. Burikhanov, R. *et al. Cell Reports* **6**, 271–277 (2014).
12. Satelli, A. & Shulin, L. *Cell. Mol. Life Sci.* **68**, 3033–3046 (2011).
13. Eckes, B. *et al. J. Cell Sci.* **113**, 2455–2462 (2000).
14. Gillard, B.K., Harrell, R.G. & Marcus, D.M. *Glycobiology* **6**, 33–42 (1996).

Acknowledgments

This work was supported by National Center for Research Resources through 'COBRE Center for Biomedical Research Excellence' grant P20 RR020171 (to L. Hersh, who is the principal investigator of the study on which D.S.W. is core director), NIH–National Cancer Institute grants R01 CA60872 and R21 CA179283 (to V.M.R.) and University of Kentucky Center for Clinical and Translational Science Drug Discovery Pilot grant (to V.M.R., D.S.W. and C.L.).

Author contributions

R.B. contributed to experimental biological studies; V.M.S. contributed to arylquin organic syntheses; N.H. contributed to experimental biological studies; W.Z. contributed to experimental biological studies; W.J.L. contributed to NMR studies characterizing arylquins; A.H. contributed to computational studies; C.-G.Z. contributed to computational studies; D.S.W. contributed to the design of arylquin syntheses; C.L. contributed to biological studies of biotinylated arylquin; and V.M.R. contributed to the design of Par-4 biological studies.

Competing financial interests

The authors declare competing financial interests: details accompany the online version of the paper.

Additional information

Supplementary information, chemical compound information and chemical probe information is available in the online version of the paper. Reprints and permissions information is available online at http://www.nature.com/reprints/index.html. Correspondence and requests for materials should be addressed to V.M.R.

ONLINE METHODS

Chemistry. Nutlin-3a, an inhibitor of MDM2 that is reported to bind directly to MDM2, release, stabilize and activate p53 (ref. 10), was acquired from Cayman Chemical Company. Brefeldin A, *N*-benzyloxycarbonyl-Val-Ala-Asp(O-Me) fluoromethyl ketone(zVAD-fmk) and other chemicals were purchased from Sigma-Aldrich or Fisher Scientific or were synthesized according to procedures documented in the literature. The synthesis of Arylquin 1, which used 4-(*N*,*N*-dimethylamino)-2-aminobenzaldehyde in a Friedländer condensation with 2-fluorophenylacetonitrile[15], and of other heterocyclic families is described in the **Supplementary Note**. The condensation of 2-amino-4-(*N*,*N*-dimethylamino)benzaldehyde with 2-(2-fluorophenyl)acetyl chloride secured 7-(dimethylamino)-3-(2-fluorophenyl)quinolin-2(1H)-one, and treatment with Lawesson's reagent[16] provided 7-(dimethylamino)-3-(2-fluorophenyl) quinoline-2(1H)-thione. S-alkylation of this intermediate with (+)-biotinyl-iodoacetamidyl-3,6-dioxaoctanediamine led to biotinylated Arylquin 9 (**Supplementary Note**). Solvents were used from commercial vendors without further purification unless otherwise noted. NMR spectra were determined on a Varian instrument (^{1}H, 400MHz; ^{13}C, 100Mz). High-resolution electrospray ionization (ESI) mass spectra were recorded on a LTQ-Orbitrap Velos mass spectrometer (Thermo Fisher Scientific, Waltham, MA, USA). The FT resolution was set at 100,000 (at 400 *m*/*z*). Samples were introduced through direct infusion using a syringe pump with a flow rate of 5 µl/min. MALDI mass spectra were obtained on a Bruker Utraflexstreme time-of-flight mass spectrometer (Billerica, MA) using DHB (2,5-dihydroxybenzoic acid) matrix. The purity of compounds was established by combustion analyses by Atlantic Microlabs, Inc., Norcross, GA. Compounds were chromatographed on preparative layer Merck silica gel F254 unless otherwise indicated.

Cells and plasmids. Human lung cancer cell lines H1299, HOP92, A549 and H460; the mouse lung cancer cell line LLC1; human prostate cancer cell lines LNCaP, DU145 and PC-3; and the primary human lung fibroblast cell line HEL and the epithelial cell lines HBEC and BEAS-2B were from ATCC; the normal human prostate epithelial cell line PrE and the human prostate stromal cell line PrS were from Lonza Inc. KP7B cells were from T. Jacks (Massachusetts Institute of Technology). PC-3 MM2 cells, which were derivatives of PC-3 cells, were from S.-H. Lin (MD Anderson Cancer Center, Houston, Texas). Par-4$^{+/+}$ and Par-4$^{-/-}$ MEFs were derived from wild-type and Par-4–null C57BL/6 mice generated by Taconic[11]. Vimentin-null (Vim$^{-/-}$) and wild-type MEFs as well as vimentin-expressing (Vim^{+}) and vimentin-deficient (Vim^{-}) SW13 cells were from A. Brown (Ohio State University).

Antibodies and siRNA duplexes. Par-4 (R334; 1:800 or 1:1,000 dilution for western blots; 1:1,000 for ICC), Col1A1 (H-197, 1:1,000 dilution), Vimentin (H-84, 1:1,000 dilution) were used for western blotting or ICC. Vimentin (RV202, 1:200 dilution for ICC, and 4 µg ml^{-1} for immunoprecipitation) was used for ICC and immunoprecipitation. GRP78 (N20, 1:100 dilution for ICC, and 1:250 dilution for flow cytometry), Col1A1 (H-197, 1:1,000 dilution), p53 (DO-1, 1:1,000 dilution) and pan-cytokeratin (C11, 1:100 dilution for ICC) antibodies were from Santa Cruz Biotechnology. Active caspase 3 antibody (Asp175; 5A1E, 1:100 dilution for ICC) and p53 antibody (1C12, 1:1,000 dilution) were from Cell Signaling. The β-actin antibody (clone AC-74, 1:8,000 dilution) was from Sigma Chemical Corp.

Pulldown experiments. To identify the target protein for compound Arylquin 1, pulldown experiments were performed as described previously[17]. MEFs or HEL cells (grown to confluence in 15-cm plates) were lysed in 50 ml lysis buffer (40 mM Hepes, pH 7.8, 140 mM NaCl, 10 mM NaF, 10% glycerol, 1 mM EDTA, 1% Triton 100), and the lysates were precleared at 4 °C for 1 h with 100 µl streptavidin beads (Novagen, Strep-Tactin Superflow Agarose). Binding reactions were performed by incubating the precleared cell lysates with 50 µl beads ± 25 µg of biotinylated Arylquin 1 at 4 °C for 2 h. The beads were then washed four times with buffer (40 mM Hepes, pH 7.8, 140 mM NaCl, 10 mM NaF, 10% glycerol, 1 mM EDTA), and bound protein was eluted with 50 µl of 2.5 mM Biotin/PBS. Eluted proteins were resolved by SDS-PAGE and Coomassie blue staining.

Co-immunoprecipitation and western blot analysis. Protein extracted from cell lysates was filtered, precleared with 25 µl (bed volume) of protein G-Sepharose beads and immunoprecipitated with 1 µg of respective antibodies. The eluted proteins were resolved by SDS-PAGE and subjected to western blot analysis as described[18].

Apoptosis assays and detection of cell surface GRP78. Apoptotic nuclei were identified by immunocytochemical (ICC) analysis for active caspase-3, and nuclei were revealed by 4′,6-diamidino-2-phenylindole (DAPI) staining[5,6]. A total of three independent experiments were performed, and approximately 500 cells were scored in each experiment for apoptosis under a fluorescent microscope. Cell surface GRP78 expression on the cancer cell surface was quantified by FACS analysis in the Flow Cytometry Shared Resource Facility, Markey Cancer Center as previously described[5].

Animal experiments. C57BL/6 mice were injected via the intraperitoneal route with Arylquin 1 (10 mg/kg body weight) or corn oil vehicle, and whole-blood samples were collected 24 h later. Serum was separated from the blood samples and heated at 56 °C to inactivate complement. Aliquots of the mouse serum samples were added to the growth medium (final 20% mouse serum) of normal and cancer cells in culture and tested for induction of *ex vivo* apoptosis in cancer cells. All animal procedures were performed with University of Kentucky IACUC approval.

Computational modeling. Molecular modeling of vimentin binding with Arylquin 1 and the analogs was performed by using the previously reported computational protocol[19,20]. Briefly, each ligand was docked into the binding cavity, and the resulting poses were refined by molecular dynamics (MD) simulations. The most favorable binding mode (with the lowest binding free energy), which was identified in the docking procedure, was subjected to an MD simulation for 1 ns at 298 K and used in binding free energy calculations.

Computational methods. Each ligand was docked into the binding cavity of the vimentin structure[20] using the SABRE program[21]. The docked vimentin-ligand structure was used as an initial structure for MD simulation in water. The general procedure for carrying out the MD simulations in water was essentially the same as that used in our previously reported computational studies[22,23]. Briefly, the MD simulations were performed using the Sander module from Amber12 (ref. 24). The vimentin-ligand binding complex was neutralized by adding counter ions and was solvated in an orthorhombic box of TIP3P water molecules with a minimum solute-wall distance of 10 Å. The solvated systems were energy minimized and carefully equilibrated. These systems were gradually heated from T = 10 K to T = 298.15 K in 50 ps before the production MD run. The MD simulations were performed with a periodic boundary condition in the NPT ensemble at T = 298.15 K using the Berendsen temperature coupling[25] and constant pressure (P = 1 atm) with isotropic molecule-based scaling. A time step of 2 fs was used, with a cutoff of 12 Å for the nonbonded interactions, and the SHAKE algorithm was used to keep all of the covalent bonds involving hydrogen atoms rigid[26]. Long-range interactions were handled using the particle mesh Ewald (PME) algorithm[27]. During the energy minimization and MD simulation, only the ligand and residue side chains in the binding pocket were permitted to move. A residue-based cutoff of 12 Å was used for noncovalent interactions. The production MD simulation was then carried out for 1 ns, and we made sure that the MD trajectory was stable. During the simulation, the atomic coordinates of the system were collected every 1 ps. The last 50 snapshots of the simulated structure of the MD trajectory were used to carry out the molecular mechanics with generalized Born and surface area solvation (MM/GBSA) binding energy calculations. The MM/GBSA binding energy calculations were performed by using the MM/GBSA method implemented in Amber12 (ref. 24). Our MM/GBSA calculation for each snapshot was carried out in the same way as we did for other protein-ligand systems[28]. The entropic contribution ($-T\Delta S$) was neglected in the binding free energy calculations for several reasons: (i) the calculation of the entropic contribution ($-T\Delta S$) to the binding free energy would require some additional approximations, (ii) we only needed to have a rough estimate of the relative binding free energies in this study and (iii) the $-T\Delta S$ values for all of the ligands examined in this study are expected to be close to each other and, thus, are not expected to change the order of the calculated binding energies.

Statistical analysis. All of the experiments were performed in triplicate to verify the reproducibility of the findings. The results show a mean of at least

doi:10.1038/nchembio.1631

three experiments ±s.d. Statistical analyses were carried out with Statistical Analysis System software (SAS Institute, Cary, NC), and *P* values were calculated using the Student *t*-test. The effect of interaction between two different treatments was analyzed using a two-way ANOVA model with data normality and equality of variance assumptions.

15. Amberg, W. *et al.* World Intellectual Property Organization, PCT WO2007022946 A1 20070301 (2007).
16. Lecher, H.Z., Greenwood, R.A., Whitehouse, K.C. & Chao, T.H. *J. Am. Chem. Soc.* **78**, 5018–5022 (1956).
17. Zhang, W. *et al. ACS Chem. Biol.* **8**, 796–803 (2013).
18. Goswami, A. *et al. Cancer Res.* **68**, 6190–6198 (2008).
19. Bargagna-Mohan, P. *et al. J. Biol. Chem.* **285**, 7657–7669 (2010).
20. Bargagna-Mohan, P. *et al. Chem. Biol.* **14**, 623–634 (2007).
21. Hamza, A. *et al. J. Chem. Inf. Model.* **54**, 1166–1173 (2014).
22. Hamza, A. & Zhan, C.-G. *J. Phys. Chem. B* **113**, 2896–2908 (2009).
23. Zhang, T. *et al. Mol. Cancer Ther.* **7**, 162–170 (2008).
24. Case, D.A. *et al. AMBER 12*. University of California, San Fransisco, (2012).
25. Berendsen, H.J.C., Postma, J.P.M., Vangunsteren, W.F., Dinola, A. & Haak, J.R. *J. Chem. Phys.* **81**, 3684–3690 (1984).
26. Ryckaert, J.P., Ciccotti, G. & Berendsen, H.J.C. *J. Comput. Phys.* **23**, 327–341 (1977).
27. Darden, T., York, D. & Pedersen, L. *J. Chem. Phys.* **98**, 10089–10092 (1993).
28. Hamza, A. *et al. J. Phys. Chem. B* **114**, 5605–5616 (2010).